Available online at www.sciencedirect.com
SCIENCE DIRECT®
Journal of Magnetism and Magnetic Materials 302 (2006) 190–195
www.elsevier.com/locate/jmmm

Finite size effects on the structural and magnetic properties of sol–gel synthesized $NiFe_2O_4$ powders

Mathew George[a,*], Asha Mary John[a], Swapna S. Nair[a], P.A. Joy[b], M.R. Anantharaman[a]

[a]*Department of Physics, Cochin University of Science and Technology, Cochin-682 022, India*
[b]*Physical Chemistry Division, National Chemical Laboratory, Pune-411 008, India*

Received 3 September 2004; received in revised form 19 May 2005
Available online 10 October 2005

Abstract

Nanoparticles of nickel ferrite have been synthesized by the sol–gel method and the effect of grain size on its structural and magnetic properties have been studied in detail. X-ray diffraction (XRD) studies revealed that all the samples are single phasic possessing the inverse spinel structure. Grain size of the sol–gel synthesized powders has been determined from the XRD data and the strain graph. A grain size of 9 nm was observed for the as prepared powders of $NiFe_2O_4$ obtained through the sol–gel method. It was also observed that strain was induced during the firing process. Magnetization measurements have been carried out on all the samples prepared in the present series. It was found that the specific magnetization of the nanosized $NiFe_2O_4$ powders was lower than that of the corresponding coarse-grained counterparts and decreased with a decrease in grain size. The coercivity of the sol–gel synthesized $NiFe_2O_4$ nanoparticles attained a maximum value when the grain size was 15 nm and then decreased as the grain size was increased further.

Keywords: Nanoparticles; Nickel ferrite; Grain size; Strain; Magnetic properties

1. Introduction

Synthesis of advanced ceramics as nanoparticles is currently gaining widespread interest in material processing technology [1–5]. Owing to the extremely small dimensions of nanostructured materials, a major portion of the atoms lie at the grain boundaries, which in turn is responsible for superior magnetic, dielectric and mechanical properties in these materials compared to their conventional coarse grained counterparts [6–8]. The different chemical processes currently in vogue for the synthesis of nanoparticles include co-precipitation [9], combustion method [10], sol–gel process [11], spray pyrolysis [12], micro emulsion technique [13] and hydrothermal process [14]. Among these methods, sol–gel process allows good control of the structural and magnetic properties of ceramic materials. The advantages of this method include processing at low temperatures, mixing at the molecular level and fabrication of novel materials.

Nanosized magnetic particles exhibit unique properties and have promising technological applications in high-density recording, colour imaging, ferrofluids, high-frequency devices and magnetic refrigerators [15,16]. Nanoparticles of magnetic ceramic materials are also widely used as contrasting agents in magnetic resonance imaging (MRI), replacement of radioactive materials used as tracers and delivery of drugs to specific areas of the body. From the application point of view, the most significant properties of magnetic ceramic materials, namely magnetic saturation, coercivity, magnetization and loss, change drastically as the size of the particles move down into the nanometric range [17–19]. Among the different ferrites, which form a major constituent of magnetic ceramic materials, nanosized nickel ferrite possess attractive properties for application as soft magnets and low loss materials at high frequencies [20]. Moreover, there are numerous reports wherein anomaly has been reported in the structural and magnetic properties of spinel ferrites in the nanoscale [21–23]. A typical example is zinc ferrite, which is

*Corresponding author. Tel.: +91 484 257 7404; fax: +91 484 257 7535.
E-mail addresses: m.george@cusat.ac.in (M. George), mraiyer@yahoo.com (M.R. Anantharaman).

0304-8853/$ - see front matter © 2005 Elsevier B.V. All rights reserved.
doi:10.1016/j.jmmm.2005.08.029

a normal spinel exhibiting antiferromagnetism with a Neel temperature of ~10.5 K in the micron regime [24]. However, nanoparticles of zinc ferrite prepared by different techniques show ferrimagnetic characteristics with ordering temperatures above room temperature. Nickel ferrite in the ultrafine form, is an inverse spinel exhibiting noncollinear spin structure and the magnetic moment at low temperatures is appreciably lower than the value for the bulk material [25]. Chinnasamy et al. found a mixed spinel structure for nickel ferrite when the grain size is reduced to a few nanometers [26]. They deducted this with the help of Mössbauer spectroscopy, magnetization and EXAFS. They observed that in addition to the canting of surface spins because of the broken exchange bonds, the core spins could also have canted spin structure, resulting from the occupation of the tetrahedral sites by Ni^{2+} ions. Kodama et al. [27–28] observed anomalous magnetic properties for their organic coated nickel ferrite nanoparticles. Hence, the synthesis of nickel ferrite as nanoparticles and the investigation of their various physical properties depending on the grain size continue to be an active area of research in the field of material science.

In the present investigation, nickel ferrite was prepared by sol–gel technique and they were heat treated at different temperatures to synthesize magnetic particles with varying grain size and study the finite size effects of their magnetic properties. To the best of our knowledge, such a study has seldom been reported in sol–gel derived samples in which there is a higher degree of crystallinity than in the co-precipitated samples.

2. Experimental techniques

2.1. Synthesis techniques

Phase pure $NiFe_2O_4$ has been prepared by sol–gel technique taking $Fe(NO_3)_3 \cdot 9H_2O$ and $Ni(NO_3)_2 \cdot 6H_2O$ in a 2:1 ratio and dissolving them in ethylene glycol at about 40 °C. After heating the sol of the metal compounds to around 60 °C a wet gel is obtained. The obtained gel when dried at about 100 °C self ignites to give the desired product. The samples were also fired at 300, 600 and 900 °C for 12 h.

2.2. X-ray diffraction studies

The structural characterization of all the four samples were carried out by the X-ray diffraction (XRD) technique on a Rigaku D_{max} 2C diffractometer with nickel filter using Cu-Kα radiation (wavelength $\lambda = 1.5418$ Å). The lattice parameters were calculated from the XRD data assuming the cubic symmetry.

2.3. Grain size and strain measurement

The grain size and/or microstrain developed during the synthesis process and the firing process was calculated from the line width (FWHM) (in radians) of the powder XRD lines as given below.

The measured integral line width (β) is given by

$$\beta = \beta' + \beta'' = \lambda/D \cos\theta + 4\varepsilon \tan\theta, \quad (1)$$

where β' and β'' are the contributions of grain size and strain, respectively, to line broadening, θ is the Bragg angle, ε is the strain and D is the grain size. When the strain term ($\beta'' = 4\varepsilon \tan\theta$) is negligible, ε could be evaluated, using β, the integral line width is measured for different XRD lines corresponding to different planes and Eq. (1) may be rewritten as

$$\beta \cos\theta = \varepsilon(4 \sin\theta) + \lambda/D. \quad (2)$$

This gives an equation of a straight line between $\beta \cos\theta$ and $4 \sin\theta$· Plotting $\beta \cos\theta$ (y-axis) and $4 \sin\theta$ (x-axis), the slope of the line gives the strain (ε) and the grain size (D) can be calculated from the intercept ($= \lambda/D$) of this line on the y-axis.

Assuming all the particles to be spherical, the specific surface area was calculated from the relation

$$S = 6000/D\rho, \quad (3)$$

where D is the diameter of the particle in nm and 'ρ' the density of the particle in g/cm^3.

2.4. Magnetic measurements

Magnetic measurements were carried out using a Vibrating Sample Magnetometer (EG & G PAR 4500) which can go up to a magnetic field of 20,000 Oe for all the four samples at room temperature (300 K) and liquid nitrogen temperature (80 K). The various magnetic properties like saturation magnetization and coercivity were elucidated from the hysteresis curve.

3. Results and discussions

The XRD pattern of all the four samples of $NiFe_2O_4$ powders synthesized by the sol–gel technique is depicted in Fig. 1. All the characteristic peaks of $NiFe_2O_4$ are present in the diffraction pattern. The XRD data agrees well with the standard JCPDS values [29]. However, a sharp increase in the crystalline nature of the nickel ferrite powders is observed as the firing temperature was increased which is recorded as a decrease in the broadening of the peaks in the diffraction pattern. This clearly indicates that the grain size has increased with increase of firing temperature. The grain size of the four samples heated at different temperatures is calculated using Eq. (2).

Fig. 2 shows the variation of grain size calculated using Debye Scherrer's formula and the specific surface area with firing temperature for all the four samples. From Fig. 2, it is clear that the grain size increases with increase of firing temperature. It is also observed that the value of D determined from XRD lines at different θ values differs, indicating the presence of strain. Hence, Eq. (2) is used to

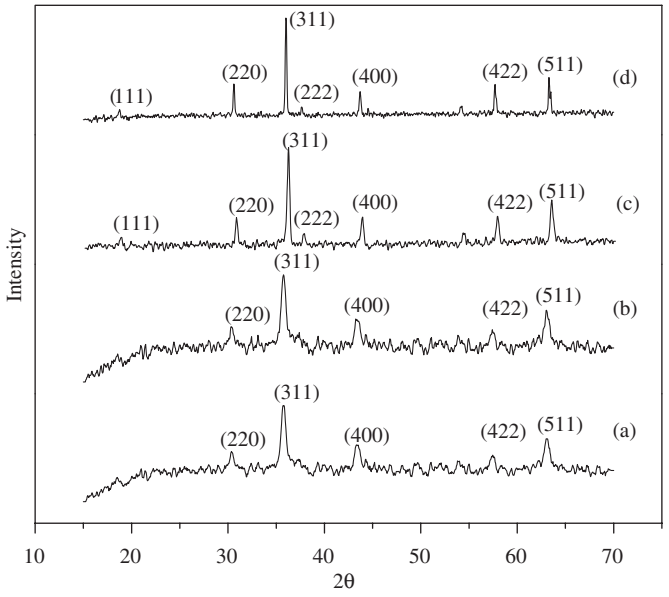

Fig. 1. XRD pattern of the (a) as prepared $NiFe_2O_4$ powder, (b) the $NiFe_2O_4$ powder heated at 300 °C, (c) at 600 °C and (d) 900 °C all for a duration of 12 h.

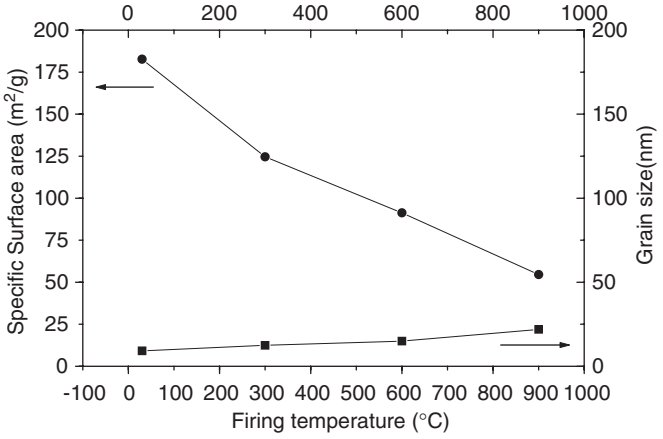

Fig. 2. Variation of grain size and specific surface area with firing temperature for the sol–gel synthesized $NiFe_2O_4$.

calculate the grain size and the strain factor from the line width values. The specific surface area was calculated using Eq. (3). It was found that the specific surface area of the particles decreases as the firing temperature increases, indicating the increase of grain size.

Fig. 3 shows the strain measurements for all the four sol–gel synthesized $NiFe_2O_4$. It was observed that the variation of $4\sin\theta$ with $\beta\cos\theta$ is linear for all the samples. The straight lines obtained were extrapolated to y-axis to measure the strain as well as the grain size.

The various magnetic properties like saturation magnetization and coercivity are estimated from the hysteresis curve. Fig. 4 shows the hysteresis curve for the $NiFe_2O_4$ nanoparticles measured at 300 and at 80 K. Table 1 gives the values of saturation magnetization and coercivity of the sol–gel synthesized nickel ferrite particles with different grain sizes.

The specific saturation magnetization (σ_s) of the nanosized nickel ferrite is observed to decrease with decreasing grain size. The linear decrease in saturation magnetization is accompanied by an increase in specific surface area as shown in Fig. 5.

In the bulk $NiFe_2O_4$, Ni exhibits a strong octahedral site preference and these ferrites crystallize in the inverse spinel structure. However, in the ultrafine regime, the findings of various researchers as regard the saturation magnetization are at variance [26–30]. Some researchers have reported increase in saturation magnetization with decrease in grain size [26], while others observed a decrease in M_s with decrease in grain size [27,28].

The observed increase or decrease can be due to many factors. Cation redistribution, the existence of surface spins or the formation of spin glass structure can all influence the magnetic properties at the submicron sizes. The presence of a dead layer has also been thought to be one of the reasons for the reduced magnetization in the ultrafine regime [30]. The saturation magnetization of $NiFe_2O_4$ calculated using Neel's sublattice theory is 50 emu/g and the reported value for the bulk sample is 56 emu/g [22]. The sample fired at 900 °C shows a maximum value of 49 emu/g, which is by and large in tune with the reported values of M_s for nickel ferrite.

Several researchers [30] invoked the theory of dead layer like a core shell model to explain the reduction in magnetization with grain size reduction. In the core shell model, it is assumed that the magnetic particles are shielded inside a non-magnetic layer. However, Kodama and Berkowitz [27,28] with the help of Mössbauer spectroscopy ruled out the possibility of the existence of dead layer in magnetization. Also cation redistribution can be a reason for anomalous results in magnetization [26].

The exhibition of lower saturation magnetization at fine grain sizes can be attributed to the following. The ferrite can be thought to possess collinear ferrimagnetic structure. In the usual structural model for a ferrite the magnetization of tetrahedral (A) sublattice is antiparallel to that of octahedral (B) sublattice. However, ultrafine nickel ferrites have non-collinear magnetic structure on the surface layer [25]. The decreasing grain size causes an increase in the proportion of non-collinear magnetic structure, in which magnetic moments are not aligned with the direction of external magnetic field. This increase in the proportion of non-collinear structure decreases the saturation magnetization.

In ultrafine particles, surface to volume ratio becomes so large that the surface becomes predominant in the determination of the characteristics. Thus in our system, the small grained magnetic particles possess lower saturation magnetization, and it increases with the increase in grain size. In the as prepared samples, the low-magnetization value is accounted for by the higher amount of non-collinear surface spins that is present in the surface of the ultrafine particles. As the grain size increases, this

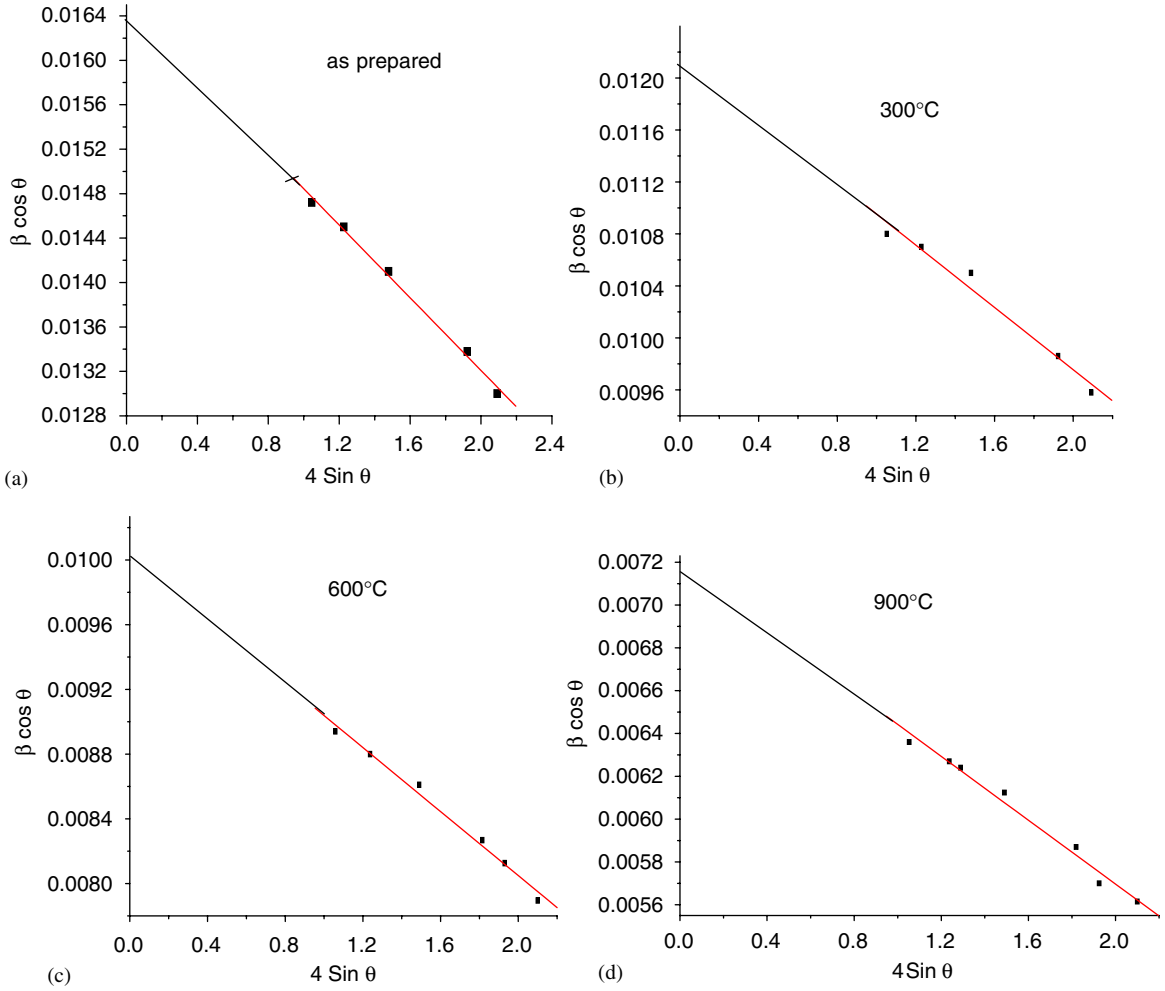

Fig. 3. Strain graphs for the sol–gel synthesized (a) as prepared $NiFe_2O_4$ (b) $NiFe_2O_4$ sample heated at 300 °C (c) 600 °C and (d) 900 °C all for a duration of 12 h.

contribution becomes less and thus the magnetization value reaches the theoretical limit as per Neel's two sub lattice model.

Fig. 6 shows the variation of coercivity with average grain size of the sol–gel synthesized nickel ferrite at 300 and at 80 K. It is evident from the graph that as the grain size increases, the value of coercivity increases, reaches a maximum value and then decreases at room temperature as well as at 80 K. This variation of H_c with grain size can be explained on the basis of domain structure, critical diameter and the anisotropy of the crystal [31–33]. A crystallite will spontaneously break up into a number of domains in order to reduce the large magnetization energy it would have if it were a single domain. The ratio of the energies before and after division into domains varied as $\sqrt{D}$, where 'D' is the particle diameter. Thus as 'D' becomes smaller, the reduction in energy becomes smaller and this suggests that for very small D the crystallite prefers to remain in the single domain.

In the single domain region as the grain size decreases the coercivity decreases because of thermal effects. The coercivity H_c in the single domain region is expressed as

$$H_c = g - \frac{h}{D^2}, \tag{4}$$

where g and h are constants.

In the multi domain region the variation of coercivity with grain size can be expressed as in [32],

$$H_c = a + \frac{b}{D}, \tag{5}$$

where 'a' and 'b' are constants and 'D' is the diameter of the particle. Hence in the multi domain region the coercivity decreases as the particle diameter increases. For magnetic nanoparticles having no interaction between them, the coercivity H_c is given by [34].

$$H_c = H_{co}\left(1 - \frac{T}{T_B}\right)^{1/2}, \tag{6}$$

where H_{co} is the coercivity at $T = 0$ K, T the temperature of measurement and T_B the critical blocking temperature,

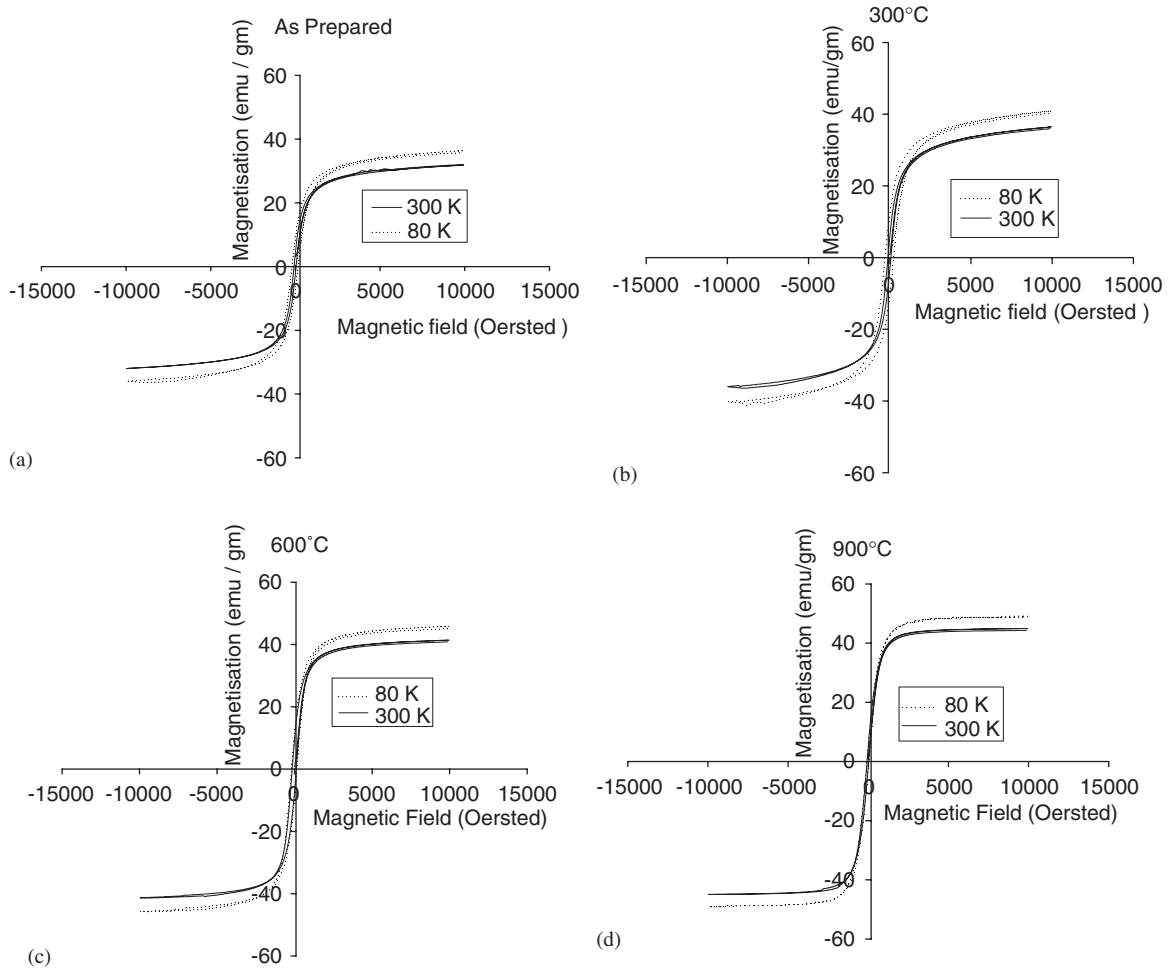

Fig. 4. Hysteresis curve (a) as prepared $NiFe_2O_4$ powder (b) $NiFe_2O_4$ powder heat treated at 300 °C (c) 600 °C and (d) 900 °C measured at room temperature and at 80 K.

Table 1
Magnetization paraers of sol–gel synthesized $NiFe_2O_4$

Grain size (nm)	Saturation magnetization (M_s) (emu/gm)		Coercivity (H_c) (Oersted)	
	300 K	80 K	300 K	80 K
9.17	32.1	36.2	59	183
12.44	36.2	40.6	90	263
14.94	41.2	45.4	130	172
21.95	44.7	49.1	50	65

below which hysteresis appears and superparamagnetism disappears and this explains the decrease of coercivity of nanonickel ferrites as the temperature increases.

It can be seen that for $NiFe_2O_4$, a critical grain size 15 nm is obtained at 300 K. At the same time the variation of H_c with grain size at 80 K though similar, has a different critical size, of 13 nm corresponding to the formation of single domain particles. This behaviour is in accordance

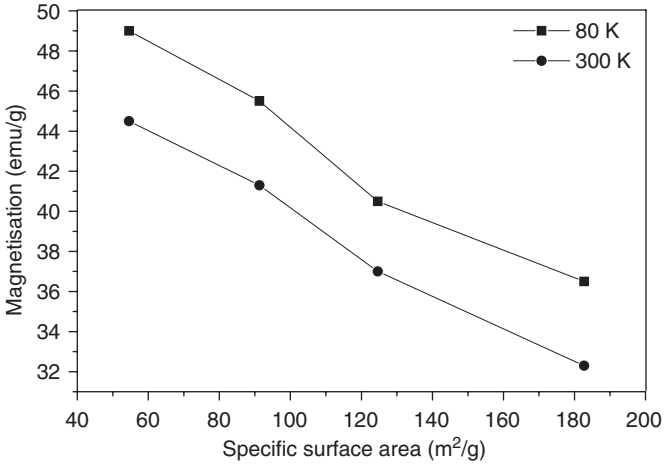

Fig. 5. Variation of saturation magnetization with specific surface area for $NiFe_2O_4$.

with the equation [32]

$$\left(\frac{D_S}{D}\right)^{3/2} = \left(\frac{T}{T_B}\right)^{1/2}. \quad (7)$$

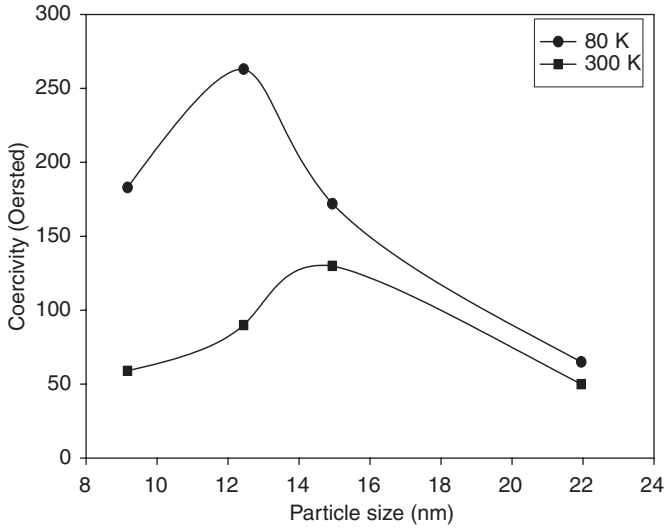

Fig. 6. Variation of coercivity with grain size for the sol–gel synthesized $NiFe_2O_4$.

According to Eq. (7) as the temperature of measurement (T) decreases, the critical grain size (D_s) of the fine particles decrease. Hence in Fig. 6, the peak value of coercivity has got shifted to the lower grain size region when the temperature decreases from 300 to 80 K. This clarifies the decrease of the critical grain size of the ultra fine nickel ferrites as the temperature of measurements decreases from 300 to 80 K.

4. Conclusion

The XRD studies of the sol–gel synthesized $NiFe_2O_4$ showed that it has the inverse spinel structure and the X-ray data agreed well with the reported data. It was observed that in addition to a change in the grain size, strain is also induced during the firing process. The magnetic studies carried out using the Vibrating Sample Magnetometer showed that the specific saturation magnetization (σ_s) of the nanosized $NiFe_2O_4$ decreased as the grain size decreased. As the grain size was increased by the annealing process, the coercivity was found to increase, attain a maximum value and then decrease. The nanosized particles of $NiFe_2O_4$ synthesized by the sol–gel method could be sintered at a lower temperature when compared to its solid-state counterpart. The sintering behaviour of $NiFe_2O_4$ nanoparticles is much superior compared to coarse-grained powder obtained through the solid-state reaction process.

Acknowledgments

MG thanks the University Grants Commission, Government of India for the fellowship. MRA and SSN acknowledge financial assistance provided by DST (File No SP-S2-M-64/96). AMJ is grateful for the financial assistance offered in the form of a post doctoral fellowship in Nanoscience and Nanotechnology by DST, Govt of India.

References

[1] G. Skandan, Y.J. Chen, N. Glumac, B.H. Kear, Nanostruct. Mater. 11 (1999) 149.
[2] D. Ravichandran, R. Roy, P. Ravindrananthan, W.B. White, J. Am. Ceram. Soc. 82 (1999) 1082.
[3] T. Tsuzuki, P.G. McCormick, Acta Mater. 48 (2000) 2795.
[4] J.G. Li, X.D. Sun, Acta Mater. 48 (2000) 3101.
[5] B.L. Shen, T. Itoi, T. Yamasaki, Y. Ogino, Scripta Mater. 42 (2000) 893.
[6] H.J. Hoffler, R.S. Averback, Scripta Metall. Mater. 24 (1990) 240.
[7] I.E. Candlish, B.H. Kear, B.K. Kim, Nanostruct. Mater. 1 (1992) 119.
[8] G. Skandan, H. Hahn, M. Roddy, W.R. Cannon, J. Am. Ceram. Soc. 77 (1994) 1706.
[9] D.H. Chen, Y.Y. Chen, J. Colloid Interface Sci. 9 (2001) 235.
[10] J.J. Kingsley, K. Suresh, K.C. Patil, J. Mater. Sci. 25 (1990) 1305.
[11] D.H. Chen, X.R. He, Bull. Mater.Res. 36 (2001) 1369.
[12] S.Z. Zhang, G.L. Messing, J. Am. Ceram. Soc. 73 (1990) 61.
[13] D.H. Chen, Y.Y. Chen, J. Colloid Interface Sci. 41 (2001) 236.
[14] S. Komarneni, M.C. D'Arrigo, C. Leonelli, G.C. Pellacani, H. Katsuki, J. Am. Ceram. Soc. 81 (1998) 3041.
[15] J.L. Dorman, D. Fiorani (Eds), Magnetic Properties of Fine Particles, North-Holland, Amesterdam.
[16] M. Kishimoto, Y. Sakurai, T. Ajima, J. Appl. Phys. 76 (1994) 7506.
[17] I.M.L. Billas, A. Chatelain, W.A. de Heer, Science 265 (1994) 1682.
[18] D.D. Awschalom, D.P.D. Vincenzo, Physics Today 43, (1995).
[19] J. Shi, S. Gider, K. Babcock, D.D. Awschalom, Science 271 (1996) 937.
[20] S. Son, M. Taheri, E. Carpenter, V.G. Harris, M.E. McHenry, J. Appl. Phys. 91 (10) (2002) 7589.
[21] H. Ehrhardt, S.J. Campbell, M. Hofmann, J. Alloys Compounds 339 (2002) 255.
[22] V. Sepelak, K. Tkacova, V.V. Boldyrev, S. Wibmann, K.D. Becker, Physica B 617 (1997) 234.
[23] Qi Chen, Z. John Zhang, Appl. Phys. Lett. 73 (1998) 3156.
[24] S.D. Shenoy, P.A. Joy, M.R. Anantharaman, J. Magn. Magn. Mater. 269 (2004) 217.
[25] A.H. Morrish, K. Haneeda, J. Appl. Phys. 52 (1981) 2496.
[26] C.N. Chinnasamy, A. Narayannasamy, N. Ponpandian, K. Chatopadhyay, K. Shinoda, B. Jeyaadevan, K. Tohji, K. Nakatsuka, T. Furubayashi, I. Nakatani, Phy. Rev B 63 (2001) 184108.
[27] R.H. Kodama, A.E. Berkowitz, E.J. McNiff, S. Foner, Phy. Rev. Lett. 77 (1996) 394.
[28] R.H. Kodama, A.E. Berkowitz, Phy. Rev. B 59 (1999) 6321.
[29] ASTM 10-325 (Ni-ferrite) Nat. Bur. Stands (U.S) cir. 539-1044 (1960).
[30] M. Zheng, X.C. Wu, B.S. Zou, Y.J. Wang, J. Magn. Magn. Mater. 183 (1998) 152.
[31] George C. Hadjipanayis, Richard W.Siegel (Eds.), Nanophase Materials–Synthesis-Properties-Applications, Kluwer Academic Publishers, Drodrecht.
[32] B.D. Cullity, Introduction to Magnetic Materials, Addison-Wesely Publishing Company. Inc, Reading, MA, 1972.
[33] S. Chikazumi, Physics of Magnetism, Wiley, New York, 1959.
[34] S. Banerjee, S. Roy, J.W. Chen, D. Chakravorty, J. Magn. Magn. Mater 219 (2000) 45.